ELSEVIER

Inorganica Chimica Acta 229 (1995) 373–382

Inorganica Chimica Acta

Acetonitrile complexes of diiridium Part 1. Isolation and characterization of the partially solvated cations $[Ir_2(COD)(\mu\text{-form})_2(MeCN)_3]^{2+}$ and $[Ir_2(\mu\text{-form})_2(MeCN)_6]^{2+}$ (COD = 1,5-cyclooctadiene, form = *N,N'*-di-*p*-tolylformamidinate) ☆

Kim R. Dunbar *, Shannon O. Majors, Jui-Sui Sun

Department of Chemistry, Michigan State University, East Lansing, MI 48824, USA

Received 15 July 1994; revised 22 August 1994

Abstract

Two partially solvated dinuclear complexes of the Ir_2^{4+} core have been prepared from reactions of $Ir_2(COD)(\mu\text{-form})_2(O_2CCF_3)_2(H_2O)$ (**1**) with an alkylating reagent in acetonitrile. The compound $[Ir_2(COD)(\mu\text{-form})_2(MeCN)_3][BF_4]_2$ (**2**) is produced in essentially quantitative yields from reactions of **1** with an excess of Et_3OBF_4 in acetonitrile at room temperature whereas the thermal substitution product $[Ir_2(\mu\text{-form})_2(MeCN)_6][BF_4]_2$ (**3**) is isolated in ~60% yield when the identical reaction is refluxed. Both compounds were fully characterized by IR and NMR spectroscopies, electrochemistry and X-ray crystallography. Single crystal X-ray data for $2\cdot(CH_3)_2CO\cdot(C_2H_5)_2O$: monoclinic, $P2_1/n$, $a = 19.534(6)$, $b = 13.285(5)$, $c = 22.113(4)$ Å, $\beta = 105.07(2)°$, $V = 5541(5)$ Å^3, $Z = 4$, $R = 0.074$, $R_w = 0.107$; **3**: orthorhombic, *Pbca*, $a = 21.670(6)$, $b = 31.407(5)$, $c = 14.543(6)$ Å, $V = 9898(9)$ Å^3, $Z = 8$, $R = 0.047$, $R_w = 0.053$. The molecular structure of $[Ir_2(COD)(\mu\text{-form})_2(MeCN)_3]^{2+}$ is very similar to the parent trifluoroacetate complex and consists of an Ir–Ir unit bridged by two *cis*-tolylformamidinate groups, with one Ir atom ligated by a cyclooctadiene ligand in the equatorial plane and the other Ir center ligated by three MeCN molecules. The absence of an axial ligand on the Ir center bonded to the COD ligand and the short Ir–$NCCH_3$(axial) interaction of the other Ir atom (2.02(3) Å) support the formulation of the compound as a mixed-valence Ir(I)–Ir(III) species. The more symmetrical cation $[Ir_2(\mu\text{-form})_2(MeCN)_6]^{2+}$ is comprised of *cis*-tolylformamidinate ligands and six acetonitrile molecules that occupy four equatorial and two axial sites. In spite of the presence of two bridging ligands, the cations in **2** and **3** are considerably distorted from an eclipsed geometry with average torsional twist angles χ of 28 and 20°, respectively. The Ir–Ir distances of 2.717(2) Å for (**2**) and 2.601(1) Å for (**3**) are shorter than the corresponding metal–metal interaction in the parent complex $Ir_2(COD)(\mu\text{-form})_2(O_2CCF_3)_2(H_2O)$ (2.774(1) Å) but are appreciably longer than the Ir–Ir bond length in the previously reported tetra-bridged molecule $Ir_2(\mu\text{-form})_4$ (2.524(3) Å). The ^1H NMR spectral properties of the new compounds are in accord with retention of the solid state structures in solution (C_s symmetry for **2** and C_{2v} symmetry for **3**). Electrochemical measurements of **2** and **3** performed in acetone at a glassy carbon electrode revealed quite different electronic properties for the two diiridium species, with **2** exhibiting behavior similar to the starting compound **1** which is in agreement with its description as a mixed-valence species. The syntheses and structures of the two new compounds in this study are discussed in light of their potential use as precursors to other metal–metal bonded Ir_2^{4+} complexes including bridging carboxylate compounds and a fully solvated dinuclear cation.

Keywords: Crystal structures; Iridium complexes; Acetonitrile complexes; Dinuclear complexes

1. Introduction

Homoleptic dinuclear cations of general formula $[M_2(MeCN)_n]^{4+}$ (M = Mo [1], Tc [2], Re [3], Rh [4] and $n = 8$–10) are a fascinating new class of molecules in the field of metal–metal bond chemistry. Typically, complexes that are used as starting materials in dinuclear chemistry contain anionic π-donors such as carboxylates and halides which are useful for synthesizing derivatives with other strong donor ligands, but which are generally unsuitable for preparing compounds with neutral donors; the availability of labile, solvated species opens up new possibilities for a wealth of unexplored

☆ Dedicated to Professor F.A. Cotton on the occasion of his 65th birthday.

* Corresponding author.

SSDI 0020-1693(94)04268-Z

metal–metal bond chemistry with less basic donor ligands.

We have been investigating reactions of the decakisacetonitrile dinuclear cations of Mo, Re and Rh in a variety of contexts including photochemical and materials applications [3,5]. Among these three metals, the most intriguing results to date have been unearthed in reactions of the dirhodium analog $[Rh_2(MeCN)_{10}][BF_4]_4$. In particular, it was discovered that the unbridged dirhodium unit is remarkably stable with respect to disproportionation to corresponding Rh(I) and Rh(III) mononuclear solvated species in the *absence* of strong donor ligands. Although homolytic Rh–Rh bond cleavage is induced by thermal and photochemical excitation, the resulting Rh(II)$^{\cdot}$ radicals participate in a complicated series of redox reactions, the final result of which is regeneration of the parent dinuclear Rh(II)–Rh(II) species [5d]. Trapping studies involving CO and CNR ligands support a mechanism that involves formation of Rh(I) and Rh(III) intermediates that eventually recombine to form the parent Rh_2(II,II) metal–metal bonded cation [5e].

Given the unusually high stability of the dirhodium solvated cation, our quest for additional examples of homoleptic dinuclear acetonitrile cations led quite logically to the attempted synthesis of $[Ir_2(MeCN)_{10}]^{4+}$ which, we reasoned, may be even more stable than the Rh analog due to increased overlap of the more diffuse 5d orbitals. This hypothesis notwithstanding, a formidable obstacle was immediately apparent, namely the lack of a suitable Ir–Ir singly bonded starting material. The tetraacetate compounds $M_2(O_2CCH_3)_4$ provide convenient entries into the solvated chemistry of Mo(II) and Rh(II), but unfortunately $Ir_2(O_2CR)_4$ analogs are not known to exist. In fact, the only reported example of a diiridium(II,II) compound that contains four bridging anionic ligands is $Ir_2(\mu\text{-form})_4$ (form = *N*,*N*′-di-*p*-tolylformamidinate) [6] (Scheme 1a), and although the electron count and structural characteristics of this compound are ideal for the present application, this compound is very stable and also presents a challenge to isolate in a solid form due to its high solubility. Other examples of singly-bonded diiridium(II,II) species have appeared in the literature, e.g. $[Ir_2(TMB)_4][BPh_4]_2$ (TMB = 2,5-diisocyamo-2,5-dimethylhexane) [7] (Scheme 1b), $Ir_2(Tcbiim)_2(CO)_4(MeCN)_2\{P(OEt)_3\}_2$ (Tcbiim = tetracyanobiimidazole anion) [8] (Scheme 1c), and $Ir_2(OEP)_2$ (OEP = octaethylporphyrin) [9], but they contain carbonyl, isocyanide, thiolate [10], porphyrin or pyrazolate ligands [11], none of which are particularly substitutionally labile [12].

Due to the narrow field of Ir_2(II,II) candidates from which to choose, we turned our attention to the unusual mixed-valence Ir_2(I,III) complex $Ir_2(COD)(\mu\text{-form})_2(\eta^1\text{-}O_2CCF_3)_2(H_2O)$, which was used to synthesize $Ir_2(\mu\text{-form})_4$ [13,14]. We now report the syntheses and full characterization of two *partially solvated* diiridium complexes, $[Ir_2(COD)(\mu\text{-form})_2(MeCN)_3]^{2+}$ and $[Ir_2(\mu\text{-form})_2(MeCN)_6]^{2+}$, isolated from reactions of $Ir_2(COD)(\mu\text{-form})_2(\eta^1\text{-}O_2CCF_3)_2(H_2O)$ with Et_3OBF_4 in MeCN. These compounds may be viewed as intermediates in the reaction pathway to the, as yet, elusive fully solvated diiridium cation.

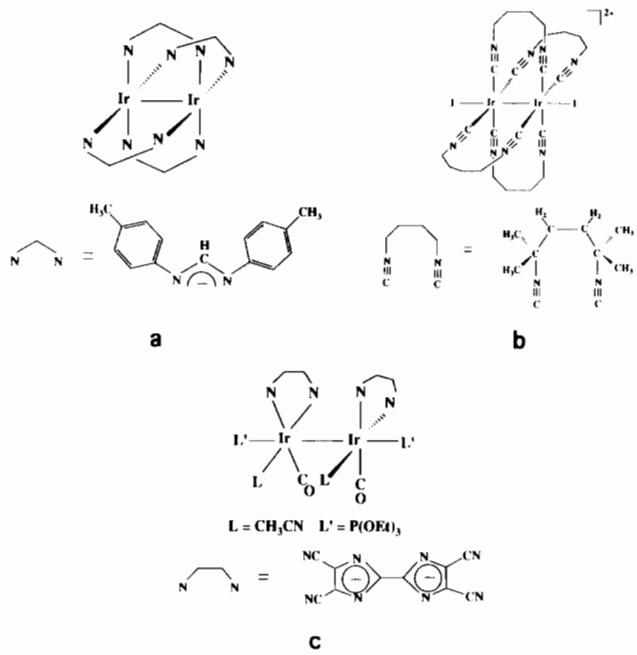

Scheme 1.

2. Experimental

2.1. Starting materials

The compound $(COD)Ir(\mu\text{-form})_2Ir(O_2CCF_3)_2(H_2O)$ [13] and the ligand *N*,*N*′-di-*p*-tolylformamidine [15] were prepared according to literature methods. The key reagents used in this study, viz. $[IrCl(COD)]_2$, $Ag(O_2CCF_3)$, and Et_3OBF_4 in CH_2Cl_2, were purchased from Aldrich and used as received. Acetonitrile, acetone and diethyl ether were freshly distilled from CaH_2, 3 Å molecular sieves and sodium/potassium benzophenone ketyl, respectively.

2.2. Reaction procedures

All operations were carried out under an argon atmosphere by using standard Schlenk-line techniques. To remove trace amounts of oxygen, the argon was passed through a catalyst column packed with manganous oxide supported on silica gel that had been activated at 300 °C in a stream of H_2(g).

2.3. Preparation of $[(COD)Ir(\mu\text{-form})_2Ir(MeCN)_3][BF_4]_2$ (2)

A quantity of $(COD)Ir(\mu\text{-form})_2Ir(O_2CCF_3)_2(H_2O)$ (**1**) (0.207 g, 0.178 mmol) was dissolved in 10 ml of dry MeCN, treated with Et_3OBF_4 (1.1 ml) and stirred at room temperature for 0.5 h. During this time, the red–brown solution noticeably changed to a dark red hue. A dynamic vacuum was applied to evaporate the solution to a dark red residue which was then dissolved in acetone (10 ml) and treated with diethyl ether (40 ml) to precipitate a dark red microcrystalline solid. The product was collected on a fine frit by anaerobic filtration and dried in vacuo. Yield 0.191 g, 97%. Although %C, %H and %N analyses were performed on recrystallized samples, the results were consistently low, which is attributed to loss of axial MeCN. IR (KBr pellet, cm^{-1}) ν(C≡N): 2329w, 2297w, 2250w, 1614m, 1581s, 1505s, 1335m, 1229m, 1215m, 1061s,br, 820m, 545w, 521m, 486w, 457w. ^1H NMR (CD_3CN, 300 MHz) δ (ppm): 7.90 (singlet, 2H, N–CH–N); 7.19, 7.16 (overlapping doublet of doublets, 8H, aromatic-tolyl); 7.04 (doublet, 4H, aromatic-tolyl); 6.90 (doublet, 4H, aromatic-tolyl); 5.26 (singlet, broad, 2H, olefinic COD); 4.75 (singlet, broad, 2H, olefinic COD); 2.87 (singlet, 6H, eq-MeCN); 2.35–2.60 (mult, 8H, aliphatic COD); 2.33 (singlet, 6H, CH_3-tolyl); 2.29 (singlet, 6H, CH_3-tolyl); 2.14 (H_2O impurity in CD_3CN); 1.96 (singlet, 3H, free MeCN). UV–Vis (MeCN) λ_{max} (nm) (ϵ (M^{-1} cm^{-1})): 783 (647), 450 (3.29×10^3), 450(sh), 255 (3.96×10^4). Cyclic voltammetry ($(CH_3)_2CO$): $E_{1/2}$(ox) = +1.23 V, $E_{1/2}$(red) = −0.50 V, $E_{p,c}$ = −0.15 V, $E_{p,a}$ = +1.05 V versus Ag/AgCl.

2.4. Preparation of $[Ir_2(\mu\text{-form})_2(MeCN)_6][BF_4]_2$ (3)

A sample of $(COD)Ir(\mu\text{-form})_2Ir(O_2CCF_3)_2(H_2O)$ (0.189 g, 0.162 mmol) was dissolved in 10 ml of dry MeCN and treated with 1.0 ml of Et_3OBF_4. After addition of the alkylating agent, the reaction was refluxed for 8 h during which time the dark red solution of the intermediate compound, $[(COD)Ir(\mu\text{-form})_2Ir(MeCN)_3][BF_4]_2$ (**2**), slowly turned to a transparent yellow color. The solution was cooled to room temperature, concentrated to ~5 ml by vacuum distillation, and treated with diethyl ether (40 ml) to precipitate a yellow solid which was separated from the solution and dried in vacuo. Yield 0.100 g, 53%. *Anal.* Calc. for $B_2C_{42}F_8H_{48}N_{10}Ir_2$: C, 40.32; H, 3.87; N, 11.20. Found: C, 39.21; H, 4.03; N, 10.63%. ^1H NMR (CD_3CN, 300 MHz) δ (ppm): 7.75 (singlet, 2H, N–CH–N); 7.02 (doublet, 8H, aromatic-tolyl); 6.93 (doublet, 8H, aromatic-tolyl); 2.73 (singlet, 12H, eq-MeCN); 2.26 (singlet, 12H, CH_3-tolyl); 1.95 (singlet, 6H, free MeCN). UV–Vis (MeCN) λ_{max} (nm) (ϵ (M^{-1} cm^{-1})): 440 (1040), 359(sh), 304(sh), 259 (2.20×10^4). Cyclic voltammetry ($(CH_3)_2CO$): $E_{1/2}$(ox) = +0.77 V, $E_{p,c}$ = −0.88 V, $E_{p,a}$ = −0.44 V versus Ag/AgCl.

2.5. Physical measurements

IR spectra were recorded on a Nicolet 42 FT-IR spectrophotometer as KBr pellets. ^1H NMR spectra were measured on a Varian 300-MHz spectrometer. Chemical shifts were referenced to the residual proton impurity in acetonitrile-d_3 (1.93 ppm with respect to TMS). Elemental analyses were performed by Galbraith Laboratories. Electrochemical measurements were carried out at 22 ± 2 °C on 0.15 M tetra-n-butylammonium hexafluorophosphate ($TBAPF_6$)/$(CH_3)_2CO$ solutions by using an EG&G Princeton Applied Research model 362 scanning potentiostat in conjunction with a BAS model RXY recorder. The electrodes employed were a BAS glassy carbon working electrode, an aqueous Ag/AgCl reference electrode and a Pt wire auxiliary electrode. The scan rate was 200 mV s^{-1}. The ferrocene/ferrocenium couple occurs at +0.45 V under the same conditions.

2.6. Single crystals X-ray studies

Structures were determined by application of general procedures that have been fully described elsewhere [16]. Crystallographic data for **2**·$(CH_3)_2CO$·$(C_2H_5)_2O$ and **3** were collected on a Rigaku AFC6S diffractometer with monochromated Mo Kα (λ_α = 0.71069 Å) radiation. All data were corrected for Lorentz and polarization effects. Calculations were performed on a VAXstation 4000 computer by using the Texsan crystallographic software package of the Molecular Structure Corporation [17]. Crystallographic data for the two compounds are compiled in Table 1 and positional parameters are listed in Tables 2 and 3.

2.6.1. $[(COD)Ir(\mu\text{-form})_2Ir(MeCN)_3][BF_4]_2$·$(CH_3)_2CO$·$(C_2H_5)_2O$ (**2**·$(CH_3)_2CO$·$(C_2H_5)_2O$)

X-ray quality crystals of **2** were obtained as a mixed acetone/diethyl ether solvate by storing a solution of the compound in an acetone/diethyl ether mixture (~1/5 vol./vol.) at −10 °C for 1 week. An orange–red crystal of dimensions 0.54×0.29×0.29 mm was selected and secured on the end of a glass fiber with a drop of viscous oil and placed on the goniometer in an N_2(g) cold stream at −100 ± 1 °C. Cell constants and an orientation matrix for data collection obtained from a least-squares refinement using the setting angles of 22 carefully centered reflections in the range $24 < 2\theta < 25°$ corresponded to a monoclinic cell. A total of 9762 data was measured at −100 ± 1 °C using the ω–2θ scan technique to a maximum 2θ value of 50°. The intensities of three representative reflections measured after every 150 reflections decreased by only 1%, nevertheless a

Table 1
Crystal data for $[Ir_2(COD)(\mu\text{-form})_2(CH_3CN)_3][BF_4]_2 \cdot (CH_3)_2CO \cdot (C_2H_5)_2O$ (**2**·$(CH_3)_2CO$·$(C_2H_5)_2O$) and $[Ir_2(\mu\text{-form})_2(CH_3CN)_6][BF_4]_2$ (**3**)

	2·$(CH_3)_2CO$·$(C_2H_5)_2O$	**3**
Formula	$Ir_2C_{51}H_{47}N_7O_2B_2F_8$	$Ir_2C_{42}H_{48}N_{10}B_2F_8$
Formula weight	1348.03	1250.95
Space group	$P2_1/n$ (No. 14)	*Pbca* (No. 61)
Systematic absences	$h0l$: $h+l=2n$ $0k0$: $k=2n$	$0kl$: $k=2n$ $h0l$: $l=2n$ $hk0$: $h=2n$
a (Å)	19.534(6)	21.670(6)
b (Å)	13.285(5)	31.407(5)
c (Å)	22.113(4)	14.543(6)
α (°)	90	90
β (°)	105.07(2)	90
γ (°)	90	90
V (Å^3)	5541(5)	9898(9)
Z	4	8
D_{calc} (g cm^{-3})	1.616	1.679
μ(Mo Kα) (cm^{-1})	48.49	54.22
Radiation (monochromated in incident beam), λ (Å)	Mo Kα, 0.71069	Mo Kα, 0.71069
Temperature (°C)	−100	−100
Transmission factors: max., min.	0.85, 1.22	0.29, 1.00
R [a]	0.074	0.047
R_w [b]	0.107	0.053

[a] $R=\Sigma||F_o|-|F_c||/\Sigma|F_o|$.
[b] $R_w=[\Sigma w(|F_o|-|F_c|)^2/\Sigma w|F_o|^2]^{1/2}$; $w=1/\sigma^2(|F_o|)$.

linear correction factor was applied to account for the small decay.

The systematic absences in the data set led to the space group choice of $P2_1/n$ (No. 14). The structure was solved by MITHRIL [19] and DIRDIF [20] structure programs and refined by full matrix least-squares refinement. During the latter stages of refinement it became apparent that the tolyl rings were experiencing some difficulty in anisotropic refinement; due to this problem as well as to the fact that the structure contains a large number of atoms, the refinement was completed with the phenyl carbon atoms treated as rigid groups and with the non-hydrogen atoms in **2** being refined anisotropically only when possible. After the non-hydrogen atoms had been refined isotropically, an absorption correction was applied using the program DIFABS which resulted in transmission factors of 0.69–1.00 [21]. Hydrogen atoms were included in calculated positions but were not refined. Two separate areas of interstitial solvent were located in the final difference Fourier maps, with one group of four peaks being defined as acetone and another group as diethyl ether. While the latter appeared in the difference map with reasonable distances and angles for five non-hydrogen atoms of diethyl ether, they repeatedly failed to refine without losing their connectivity, thus their positions were fixed for the final cycles. The last cycle of least-squares refinement included 4218 observed reflections with $F_o^2 \geq 3.00\sigma(F_o^2)$ and 290 variable parameters to give $R=0.074$ ($R_w=0.107$) and a quality-of-fit index of 2.98.

2.6.2. *$[Ir_2(\mu\text{-form})_2(MeCN)_6][BF_4]_2$ (3)*

Yellow crystals of **3** were grown from a concentrated solution of the compound in acetonitrile that had been carefully layered with Et_2O in a flame sealed 8 mm o.d. glass tube. A parallelepiped crystal of dimensions $0.38\times0.75\times0.35$ mm was mounted on the end of a glass fiber with silicone grease and placed in an N_2(g) cold stream at -100 ± 1 °C. An automatic search routine was used to locate and center 20 reflections in the range $26<2\theta<35°$ from which an orthorhombic cell was indexed. The data were collected at -100 ± 1 °C using the ω-scan technique to a maximum 2θ value of 50°. A total of 9535 reflections was collected with no decay being observed for three check reflections that were measured every 150 reflections during the course of the data collection. An empirical absorption correction based on azimuthal scans of three reflections with χ near 90° was applied which resulted in transmission factors ranging from 0.29 to 1.00.

The space group *Pbca* (No. 61) was selected on the basis of the systematic absences and successful refinement. The atoms were located by application of the MITHRIL [19] and DIRDIF [20] programs. Full matrix least-squares refinement allowed for successful anisotropic refinement of all non-hydrogen atoms; hydrogen atoms were included in calculated positions. The final cycle of refinement was based on 4219 observations with $F_o^2 \geq 3.00\sigma(F_o^2)$ and 527 variable parameters and converged with $R=0.47$ ($R_w=0.053$) and a goodness-of-fit of 1.69. The highest peak in the difference map was 3.02 e Å^{-3} and is the ghost of a metal atom.

Table 2
Atomic positional parameters and equivalent isotropic displacement parameters (Å²) and their e.s.d.s for $[Ir_2(\mu\text{-form})_2(COD)(CH_3CN)_3][BF_4]_2 \cdot (CH_3)_2CO \cdot (C_2H_5)_2O$

Atom	x	y	z	B_{eq}
Ir(1)	0.30378(7)	0.78860(9)	0.00473(6)	2.06(5)
Ir(2)	0.32224(7)	0.5860(1)	0.01360(6)	2.20(5)
N(1)	0.313(1)	0.777(2)	0.098(1)	2(1)
N(2)	0.372(1)	0.617(2)	0.106(1)	3(1)
N(3)	0.198(1)	0.758(2)	−0.010(1)	2(1)
N(4)	0.225(1)	0.602(2)	0.033(1)	1.8(5)
N(5)	0.291(1)	0.813(2)	−0.089(1)	3.2(6)
N(6)	0.408(1)	0.830(2)	0.028(1)	2.3(5)
N(7)	0.287(1)	0.939(2)	−0.000(1)	2.6(5)
C(15)	0.353(2)	0.697(2)	0.131(1)	2.8(6)
C(30)	0.180(2)	0.678(3)	0.009(1)	3.2(7)
C(31)	0.284(2)	0.844(3)	−0.136(2)	4.6(9)
C(32)	0.294(4)	0.871(5)	−0.200(3)	13(2)
C(33)	0.466(2)	0.863(2)	0.041(1)	3(1)
C(34)	0.532(2)	0.899(3)	0.056(2)	4(2)
C(35)	0.277(2)	1.017(2)	−0.007(2)	2.9(7)
C(36)	0.268(3)	1.137(4)	−0.003(2)	7(1)
C(37)	0.390(2)	0.417(2)	−0.043(1)	3(1)
C(38)	0.309(2)	0.394(3)	−0.061(2)	7(3)
C(39)	0.272(2)	0.490(2)	−0.064(2)	5(2)
C(40)	0.283(2)	0.583(2)	−0.090(1)	3(1)
C(41)	0.339(2)	0.593(3)	−0.122(1)	4(2)
C(42)	0.410(2)	0.637(3)	−0.084(1)	3(2)
C(43)	0.419(2)	0.597(2)	−0.015(1)	3(2)
C(44)	0.414(1)	0.503(2)	0.002(1)	2.2(6)
H(1)	0.2093	0.7480	0.1527	4.2
H(2)	0.1675	0.8576	0.2182	4.2
H(3)	0.3074	1.0708	0.1947	4.2
H(4)	0.3491	0.9612	0.1292	4.2
H(5)	0.3836	0.4274	0.1397	4.6
H(6)	0.4803	0.3454	0.2068	4.6
H(7)	0.5920	0.6068	0.2296	4.6
H(8)	0.4952	0.6888	0.1626	4.6
H(9)	0.3669	0.7016	0.1757	3.4
H(10)	0.2316	1.1077	0.2594	4.2
H(11)	0.1572	1.0586	0.2379	4.2
H(12)	0.2129	1.0162	0.2956	4.2
H(13)	0.1162	0.7514	−0.1250	5.0
H(14)	0.0222	0.8590	−0.1720	5.0
H(15)	0.0613	1.0262	−0.0129	5.0
H(16)	0.1553	0.9187	0.0341	5.0
H(17)	−0.0313	1.0759	−0.0995	5.0
H(18)	−0.0205	1.0505	−0.1649	5.0
H(19)	−0.0716	0.9861	−0.1375	5.0
H(20)	0.5644	0.8457	0.0701	5.1
H(21)	0.5413	0.9303	0.0207	5.1
H(22)	0.5365	0.9473	0.0888	5.1
H(23)	0.1313	0.6686	0.0055	3.8
H(24)	0.2751	0.4218	0.0523	6.2
H(25)	0.2460	0.2895	0.1113	6.2
H(26)	0.0946	0.4640	0.1545	6.2
H(27)	0.1238	0.5963	0.0955	6.2
H(28)	0.5949	0.3895	0.3037	4.6
H(29)	0.6232	0.3607	0.2466	4.6
H(30)	0.6465	0.4611	0.2818	4.6
H(31)	0.3113	1.1691	−0.0045	9.0
H(32)	0.2312	1.1589	−0.0374	9.0
H(33)	0.2571	1.1542	0.0351	9.0
H(34)	0.3208	0.9319	−0.1971	15.1
H(35)	0.3190	0.8186	−0.2144	15.1
H(36)	0.2492	0.8805	−0.2291	15.1
H(37)	0.2878	0.3296	−0.0682	8.1
H(38)	0.4224	0.3789	−0.0597	3.7
H(39)	0.3323	0.5726	−0.1643	5.3
H(40)	0.4415	0.6794	−0.0985	4.1
H(41)	0.2539	0.6392	−0.0866	3.2
H(42)	0.4261	0.4881	0.0454	2.7
H(43)	0.4300	0.6462	0.0171	3.8
H(44)	0.1114	0.2986	0.1946	6.2
H(45)	0.1335	0.2213	0.1506	6.2
H(46)	0.1890	0.2602	0.2096	6.2
H(47)	0.2337	0.4894	−0.0446	5.8
F(1)	0.357(1)	0.238(2)	0.832(1)	8(1)
F(2)	0.240(1)	0.226(2)	0.825(1)	8(1)
F(3)	0.310(1)	0.088(2)	0.855(2)	10(2)
F(4)	0.286(2)	0.136(2)	0.758(1)	11(2)
B(1)	0.298(3)	0.174(4)	0.813(2)	4(1)
F(5)	0.441(2)	0.234(2)	0.063(1)	10(2)
F(6)	0.424(2)	0.072(2)	0.078(1)	10(2)
F(7)	0.508(2)	0.166(3)	0.138(2)	15(1)
F(8)	0.399(2)	0.181(3)	0.126(2)	17(1)
B(3)	0.449(4)	0.163(6)	0.100(4)	8(2)
O(2)	0.430(3)	0.062(4)	0.637(2)	14(1)
C(45)	0.442(4)	0.040(6)	0.696(4)	13(2)
C(46)	0.392(4)	−0.027(5)	0.722(3)	13(2)
C(47)	0.490(5)	0.106(7)	0.750(4)	19(2)
O(1)	0.4873	0.2038	0.4064	27(2)
C(48)	0.4101	0.1762	0.3020	41(1)
C(49)	0.4881	0.1735	0.3373	46(1)
C(50)	0.5634	0.2414	0.4847	20(2)
C(51)	0.5821	0.1991	0.4321	35(1)
C(1)	0.283(1)	0.844(1)	0.1347(8)	3.5(3)
C(2)	0.229(1)	0.814(1)	0.161(1)	3.5(3)
C(3)	0.2042(9)	0.879(1)	0.2001(9)	3.5(3)
C(4)	0.2335(8)	0.975(1)	0.2127(7)	3.5(3)
C(5)	0.288(1)	1.005(1)	0.186(1)	3.5(3)
C(6)	0.312(1)	0.940(1)	0.147(1)	3.5(3)
C(7)	0.206(1)	1.046(2)	0.255(1)	3.5(3)
C(8)	0.430(1)	0.566(1)	0.1448(9)	3.8(3)
C(9)	0.4258(8)	0.464(1)	0.158(1)	3.8(3)
C(10)	0.483(1)	0.415(1)	0.198(1)	3.8(3)
C(11)	0.5453(8)	0.468(1)	0.2246(7)	3.8(3)
C(12)	0.5499(9)	0.570(1)	0.212(1)	3.8(3)
C(13)	0.492(1)	0.619(1)	0.172(1)	3.8(3)
C(14)	0.608(1)	0.414(2)	0.268(1)	3.8(3)
C(16)	0.145(1)	0.825(1)	−0.041(1)	4.2(3)
C(17)	0.105(1)	0.807(1)	−0.102(1)	4.2(3)
C(18)	0.049(1)	0.871(1)	−0.1301(7)	4.2(3)
C(19)	0.0328(8)	0.953(1)	−0.0968(8)	4.2(3)
C(20)	0.073(1)	0.971(1)	−0.0356(8)	4.2(3)
C(21)	0.129(1)	0.907(2)	−0.0077(8)	4.2(3)
C(22)	−0.029(1)	1.023(2)	−0.127(1)	4.2(3)
C(23)	0.202(1)	0.521(2)	0.068(1)	5.2(4)
C(24)	0.238(1)	0.430(2)	0.073(1)	5.2(4)
C(25)	0.221(1)	0.351(1)	0.108(1)	5.2(4)
C(26)	0.167(1)	0.364(1)	0.1384(8)	5.2(4)
C(27)	0.131(1)	0.455(2)	0.134(1)	5.2(4)
C(28)	0.149(1)	0.534(1)	0.099(1)	5.2(4)
C(29)	0.148(2)	0.278(2)	0.177(1)	5.2(4)

The equivalent isotropic temperature factor [18] is defined as follows: $B_{eq} = 8\pi^2/3(\sum_{i=1}^{3}\sum_{j=1}^{3} U_{ij} a_i^* a_j^* \mathbf{a}_i \cdot \mathbf{a}_j)$.

Table 3
Atomic positional parameters and equivalent isotropic displacement parameters (Å²) and their e.s.d.s for $[Ir_2(\mu\text{-form})_2(CH_3CN)_6][BF_4]_2$

Atom	x	y	z	B_{eq}
Ir(1)	0.63784(3)	0.15005(2)	0.60410(4)	1.99(3)
Ir(2)	0.56640(3)	0.14686(2)	0.46057(4)	2.01(3)
N(1)	0.6940(6)	0.1095(4)	0.531(1)	2.1(6)
N(2)	0.6167(8)	0.0939(4)	0.4271(9)	3.1(7)
N(3)	0.5863(7)	0.0999(4)	0.648(1)	2.5(7)
N(4)	0.5080(6)	0.1106(4)	0.5405(9)	2.3(6)
N(5)	0.6857(7)	0.2005(4)	0.5586(8)	2.5(7)
N(6)	0.5812(7)	0.1873(5)	0.676(1)	3.2(8)
N(7)	0.7002(6)	0.1499(4)	0.7199(8)	2.5(6)
N(8)	0.6236(7)	0.1800(4)	0.379(1)	3.0(7)
N(9)	0.5214(7)	0.2004(4)	0.4925(9)	2.7(7)
N(10)	0.5110(6)	0.1411(4)	0.3349(9)	2.8(7)
C(1)	0.7578(8)	0.1032(5)	0.560(1)	1.8(7)
C(2)	0.7733(8)	0.0736(5)	0.624(1)	2.9(9)
C(3)	0.834(1)	0.0712(6)	0.656(1)	4(1)
C(4)	0.879(1)	0.0985(7)	0.626(2)	5(1)
C(5)	0.8636(9)	0.1272(6)	0.559(1)	4(1)
C(6)	0.803(1)	0.1300(6)	0.525(1)	4(1)
C(7)	0.943(1)	0.0976(8)	0.665(2)	8(2)
C(8)	0.6727(8)	0.0879(5)	0.463(1)	2.5(8)
C(9)	0.6011(8)	0.0705(5)	0.348(1)	2.5(8)
C(10)	0.630(1)	0.0774(6)	0.264(1)	5(1)
C(11)	0.610(1)	0.0584(7)	0.185(1)	5(1)
C(12)	0.5584(9)	0.0327(6)	0.184(1)	4(1)
C(13)	0.5282(9)	0.0262(5)	0.265(1)	3(1)
C(14)	0.5493(8)	0.0449(5)	0.346(1)	2.5(8)
C(15)	0.534(1)	0.0151(7)	0.097(2)	6(1)
C(16)	0.6079(8)	0.0710(5)	0.717(1)	2.4(8)
C(17)	0.6149(9)	0.0815(6)	0.806(1)	3.0(9)
C(18)	0.634(1)	0.0526(6)	0.871(1)	4(1)
C(19)	0.650(1)	0.0111(6)	0.846(1)	4(1)
C(20)	0.643(1)	−0.0004(6)	0.756(2)	5(1)
C(21)	0.6224(9)	0.0289(5)	0.689(1)	3(1)
C(22)	0.670(1)	−0.0217(8)	0.918(2)	9(2)
C(23)	0.5324(8)	0.0906(4)	0.613(1)	2.1(7)
C(24)	0.4464(8)	0.0993(5)	0.514(1)	2.6(8)
C(25)	0.4232(9)	0.0597(6)	0.531(1)	4(1)
C(26)	0.362(1)	0.0489(6)	0.501(1)	4(1)
C(27)	0.3259(9)	0.0783(7)	0.457(1)	4(1)
C(28)	0.3505(9)	0.1190(6)	0.442(1)	4(1)
C(29)	0.4087(7)	0.1294(5)	0.472(1)	2.6(8)
C(30)	0.260(1)	0.0675(7)	0.422(1)	5(1)
C(31)	0.713(1)	0.2285(5)	0.536(1)	4(1)
C(32)	0.754(1)	0.2632(6)	0.504(2)	5(1)
C(33)	0.554(1)	0.2087(7)	0.724(1)	5(1)
C(34)	0.521(1)	0.237(1)	0.787(2)	11(2)
C(35)	0.7385(9)	0.1479(5)	0.775(1)	3.1(8)
C(36)	0.784(1)	0.1437(6)	0.847(1)	6(1)
C(37)	0.6520(9)	0.1977(7)	0.324(1)	5(1)
C(38)	0.685(1)	0.220(1)	0.255(2)	10(2)
C(39)	0.492(1)	0.2300(5)	0.505(1)	3(1)
C(40)	0.455(1)	0.2686(6)	0.521(2)	6(1)
C(41)	0.487(1)	0.1358(5)	0.268(1)	4(1)
C(42)	0.455(1)	0.1287(6)	0.182(2)	6(1)
H(1)	0.7430	0.0546	0.6474	3.5
H(2)	0.8442	0.0498	0.6991	4.6
H(3)	0.8944	0.1455	0.5352	5.0
H(4)	0.7929	0.1500	0.4781	5.0
H(5)	0.9453	0.0760	0.7107	10.1
H(6)	0.9712	0.0917	0.6173	10.1
H(7)	0.9519	0.1244	0.6919	10.1
H(8)	0.6982	0.0666	0.4363	3.1
H(9)	0.6639	0.0964	0.2620	5.5
H(10)	0.6330	0.0626	0.1303	5.6
H(11)	0.4923	0.0089	0.2669	4.2
H(12)	0.5276	0.0399	0.4017	3.0
H(13)	0.4937	0.0268	0.0859	6.7
H(14)	0.5603	0.0222	0.0479	6.7
H(15)	0.5304	−0.0149	0.1022	6.7
H(16)	0.6066	0.1100	0.8249	3.6
H(17)	0.6358	0.0608	0.9343	4.9
H(18)	0.6518	−0.0288	0.7379	5.9
H(19)	0.6186	0.0206	0.6263	4.0
H(20)	0.6407	−0.0444	0.9197	10.6
H(21)	0.7092	−0.0327	0.9021	10.6
H(22)	0.6718	−0.0086	0.9767	10.6
H(23)	0.5092	0.0683	0.6410	2.4
H(24)	0.4477	0.0391	0.5617	4.4
H(25)	0.3465	0.0211	0.5121	4.9
H(26)	0.3261	0.1394	0.4100	4.8
H(27)	0.4231	0.1577	0.4644	3.2
H(28)	0.2428	0.0918	0.3928	6.2
H(29)	0.2625	0.0447	0.3788	6.2
H(30)	0.2351	0.0592	0.4722	6.2
H(31)	0.7888	0.2651	0.5437	6.3
H(32)	0.7670	0.2575	0.4434	6.3
H(33)	0.7319	0.2894	0.5057	6.3
H(34)	0.5481	0.2562	0.8142	13.4
H(35)	0.4898	0.2517	0.7531	13.4
H(36)	0.5013	0.2199	0.8330	13.4
H(37)	0.7877	0.1147	0.8642	7.1
H(38)	0.8230	0.1537	0.8253	7.1
H(39)	0.7719	0.1601	0.8987	7.1
H(40)	0.7268	0.2129	0.2584	11.8
H(41)	0.6683	0.2125	0.1969	11.8
H(42)	0.6794	0.2498	0.2649	11.8
H(43)	0.4669	0.2812	0.5772	7.2
H(44)	0.4618	0.2881	0.4718	7.2
H(45)	0.4124	0.2613	0.5229	7.2
H(46)	0.4362	0.1545	0.1617	7.2

The equivalent isotropic temperature factor [18] is defined as follows: $B_{eq} = 8\pi^2/3(\Sigma_{i-1}^{3}\Sigma_{j-1}^{3}U_{ij}a_i^*a_j^*\mathbf{a}_i\cdot\mathbf{a}_j)$.

3. Results and discussion

3.1. Synthesis

The trifluoroacetate ligands on $Ir_2(COD)(\mu\text{-form})_2(O_2CCF_3)_2(H_2O)$ are easily replaced with MeCN in the presence of Et_3OBF_4 at room temperature to give the air-sensitive compound $[Ir_2(COD)(\mu\text{-form})_2(MeCN)_3][BF_4]_2$ (**2**) in essentially quantitative yields. The reaction can be terminated at this stage and the isolated product refluxed in MeCN to give the very stable cyclooctadiene-free product $[Ir_2(\mu\text{-form})_2(MeCN)_6][BF_4]_2$ (**3**), or, as outlined in Section 2, a more convenient one-pot synthesis can be used to obtain $[Ir_2(\mu\text{-form})_2(MeCN)_6[BF_4]_2$ directly from $Ir_2(COD)(\mu\text{-form})_2(O_2CCF_3)_2(H_2O)$ in 50–60% yields.

The possibility of synthesizing $[Ir_2(\mu\text{-form})_2(MeCN)_6][BF_4]_2$ or $[Ir_2(MeCN)_{10}]^{4+}$ directly from $[Ir_2(\mu\text{-form})_4]$ in MeCN was explored, but all attempts to effect substitution of the μ-form ligands by using HBF_4 or Et_3OBF_4 failed, with only minor quantities of starting material being isolated from oily green residues. Reactions of $[Ir_2(\mu\text{-form})_2(MeCN)_6][BF_4]_2$ with Me_3OBF_4 in refluxing acetonitrile, however, result in a gradual color change from pale yellow to orange, a reaction that is under further investigation.

3.2. Molecular structures

3.2.1. $[(COD)Ir(\mu\text{-form})_2Ir(MeCN)_3][BF_4]_2 \cdot (CH_3)_2CO \cdot (C_2H_5)_2O$ ($2 \cdot (CH_3)_2CO \cdot (C_2H_5)_2O$)

The cation $[(COD)Ir(\mu\text{-form})_2Ir(MeCN)_3]^{2+}$ in $2 \cdot (CH_3)_2CO \cdot (C_2H_5)_2O$, whose ORTEP is depicted in Fig. 1, consists of *cis*-μ-formamidinate ligands spanning the Ir–Ir unit along with one cyclooctadienyl group attached to Ir2 and three acetonitrile solvent molecules bonded to Ir1. The axial site in Ir2 is vacant, whereas the axial MeCN group at Ir1 is bonded at a distance of 2.02(3) Å, which is quite short given that it is comparable to the equatorial Ir–$NCCH_3$ distances of 2.04(2) Å which are usually ~0.2 Å shorter. Ir2 is roughly square-planar (or pyramidal if one includes the Ir–Ir vector) whereas Ir1 is pseudo-octahedral; these differences in geometry were interpreted as an indication of mixed valency for the axial pyridine derivative $(COD)Ir(\mu\text{-form})_2Ir(\eta^1\text{-}O_2CCF_3)_2(py)$ [13]. The close similarity between the molecular structures of $(COD)Ir(\mu\text{-form})_2Ir(\eta^1\text{-}O_2CCF_3)_2(py)$ and $[(COD)Ir(\mu\text{-form})_2Ir(MeCN)_3]^{2+}$ supports the formulation of the acetonitrile derivative as an Ir(I)Ir(III) species with a dative metal–metal bond. The Ir–Ir bond distance of 2.717(2) Å in $[(COD)Ir(\mu\text{-form})_2Ir(MeCN)_3]^{2+}$ is comparable to the analogous distance in $(COD)Ir(\mu\text{-form})_2Ir(\eta^1\text{-}O_2CCF_3)_2(py)$ (2.774(1) Å); both values are considerably longer than the corresponding Ir–Ir separations in $Ir_2(\mu\text{-form})_4$ or $[Ir(\mu\text{-form})_2(MeCN)_6]^{2+}$ (vide infra).

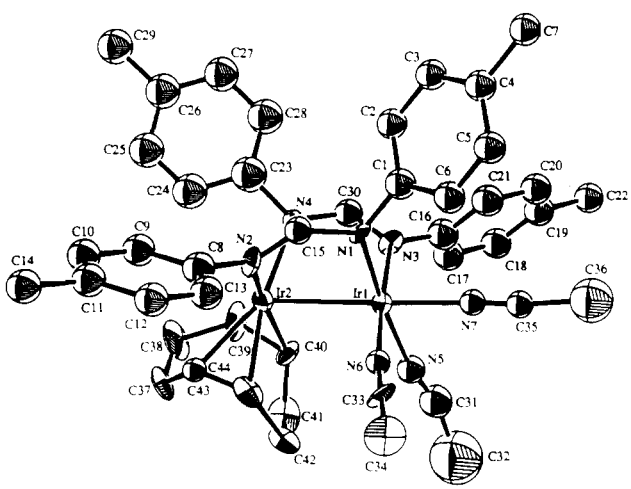

Fig. 1. ORTEP depiction of the molecular cation $[Ir_2(COD)_2(\mu\text{-form})_2(MeCN)_3]^{2+}$ in **2** with atoms represented by their 40% probability ellipsoids.

Other salient structural features of $[(COD)Ir(\mu\text{-form})_2Ir(MeCN)_3]^{2+}$ are summarized in Table 4. The average Ir–N distance and the N–CH–N angle involving the formamidinate ligands in **2** are 2.05(2) Å and 125(3)° which are not unusual. The ligand sets on Ir1 and Ir2 deviate from an eclipsed conformation as evidenced by an examination of the angles involving the Ir–Ir vector, the N atoms and the bridgehead CH group of the formamidinate ligands (see Table 6). The average twist angle χ in **2** is 28(2)° as compared to 23.3(5)° in $(COD)Ir(\mu\text{-form})_2Ir(\eta^1\text{-}O_2CCF_3)_2(py)$ [13]. In both cases, a twist about the μ-form ligands serves to relieve steric repulsions across the Ir–Ir bond and further stabilizes the metal–metal interaction without any apparent effect on the bridging ligands.

3.2.2. $[Ir_2(\mu\text{-form})_2(MeCN)_6][BF_4]_2$ (3)

The single crystal X-ray study of **3** revealed a rare, unambiguous example of an Ir(II)–Ir(II) singly bonded compound. Selected bond distances and angles and an ORTEP for **3** are provided in Table 5 and Fig. 2, respectively. Although the compound was not synthesized directly from the tetra-bridged species, the obvious relationship of $[Ir_2(\mu\text{-form})_2(MeCN)_6]^{2+}$ to $Ir_2(\mu\text{-form})_4$ warrants a comparison of the two structures. The cation $[Ir_2(\mu\text{-form})_2(MeCN)_6]^{2+}$ with C_{2v} symmetry is twisted

Table 4
Selected bond distances and angles for $2 \cdot (CH_3)_2CO \cdot (C_2H_5)_2O$

Distances (Å)			
Ir1–Ir2	2.717(2)	Ir2–C44	2.18(3)
Ir1–N1	2.04(2)	N2–C15	1.30(4)
Ir1–N3	2.04(2)	N6–C33	1.17(4)
Ir1–N5	2.04(2)	N5–C31	1.10(5)
Ir1–N6	2.05(2)	N7–C35	1.05(4)
Ir1–N7	2.02(3)	N3–C16	1.40(3)
Ir2–N2	2.06(2)	C16–C17	1.40(3)
Ir2–N4	2.07(2)	C19–C22	1.53(3)
Ir2–C39	2.15(3)	C39–C40	1.40(5)
Ir2–C40	2.21(3)	C40–C41	1.46(6)
Ir2–C43	2.16(4)		
Angles (°)			
Ir1–Ir1–N1	83.1(6)	Ir1–Ir2–C40	86.5(8)
Ir1–N5–C31	167(3)	C40–C41–C42	117(3)
Ir1–N7–C35	175(3)	C40–Ir2–C43	78(1)
Ir2–Ir1–N3	85.8(6)	N4–Ir2–C40	97(1)
Ir2–Ir1–N5	102.0(8)	N4–Ir2–C44	155(1)
Ir2–Ir1–N6	98.1(7)	Ir1–N1–C15	118(2)
Ir2–Ir1–N7	177.8(8)	Ir1–N1–C1	126(1)
N1–Ir1–N3	88.0(9)	Ir1–N3–C30	119(2)
N1–Ir1–N5	175(1)	N1–C15–N2	125(3)
N1–Ir1–N6	87.1(9)	N3–C30–N4	125(3)
N3–Ir1–N6	173(1)	N1–C1–C2	122(2)
Ir1–Ir2–N4	78.5(6)	C1–C2–C3	120(2)
Ir1–Ir2–N2	83.8(6)	C3–C4–C7	120(2)
Ir1–Ir2–C39	120.3(9)		

Table 5
Selected bond distances and angles for **3**

Distances (Å)			
Ir1–Ir2	2.601(1)	N5–C31	1.11(2)
Ir1–N1	2.05(1)	N7–C35	1.15(2)
Ir1–N3	2.03(1)	N4–C23	1.34(2)
Ir1–N5	2.01(1)	N4–C24	1.43(2)
Ir1–N6	2.00(2)	N8–C37	1.15(2)
Ir1–N7	2.16(1)	C37–C38	1.41(3)
Ir2–N2	2.05(1)	N10–C41	1.12(2)
Ir2–N4	2.06(1)	C41–C42	1.46(3)
Ir2–N8	2.00(1)	C24–C25	1.36(2)
Ir2–N9	2.00(1)	C25–C26	1.43(3)
Ir2–N10	2.19(1)	C26–C27	1.38(2)
N1–C1	1.46(2)	C27–C30	1.55(2)
N1–C8	1.29(2)		
Angles (°)			
Ir2–Ir1–N1	85.1(4)	N2–Ir2–N9	177.0(6)
Ir2–Ir1–N3	84.1(4)	Ir2–N4–C23	118(1)
Ir2–Ir1–N5	94.2(4)	Ir2–N2–C8	121(1)
Ir2–Ir1–N6	94.6(4)	Ir1–N1–C8	119(1)
Ir2–Ir1–N7	176.8(3)	Ir1–N3–C23	123(1)
N1–Ir1–N3	90.4(5)	N1–C8–N2	123(1)
N1–Ir1–N5	90.7(5)	N3–C23–N4	124(1)
N1–Ir1–N6	177.6(5)	Ir1–N1–C1	120(1)
N1–Ir1–N3	90.4(5)	N1–C1–C2	121(1)
Ir1–Ir2–N2	84.6(5)	C1–C2–C3	120(2)
Ir1–Ir2–N4	86.2(4)	C3–C4–C7	122(2)
Ir1–Ir2–N8	94.9(4)	Ir1–N7–C35	172(1)
Ir1–Ir2–N9	94.1(4)	Ir1–N5–C31	178(1)
Ir1–Ir2–N10	175.9(4)	N7–C35–C36	176(2)
N2–Ir2–N4	90.7(5)	N5–C31–C32	175(2)

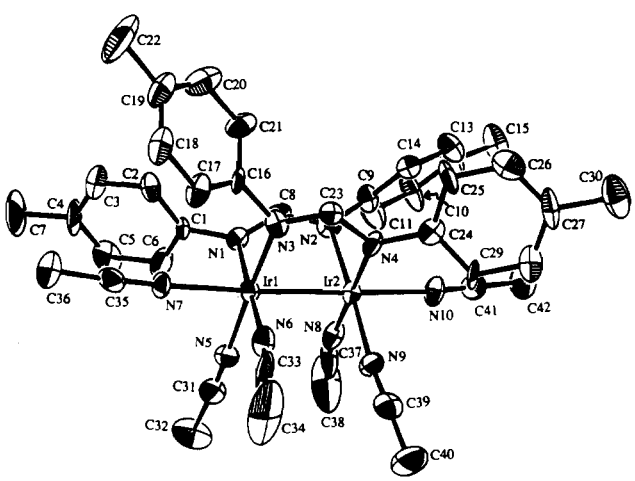

Fig. 2. ORTEP depiction of the molecular cation $[Ir_2(\mu\text{-form})_2(MeCN)_6]^{2+}$ in **3** with atoms represented by their 40% probability ellipsoids.

about the Ir–Ir vector by 20° which is intermediate between the distortion exhibited by **2** and the tetraformamidinate complex (15.6(5)°). A skeletal view of the cation in **3** looking down the Ir–Ir bond axis (Fig. 3) clearly shows the distortion from eclipsed geometry. Independent twist angles described by the formamidinate ligands and the acetonitrile groups are listed in

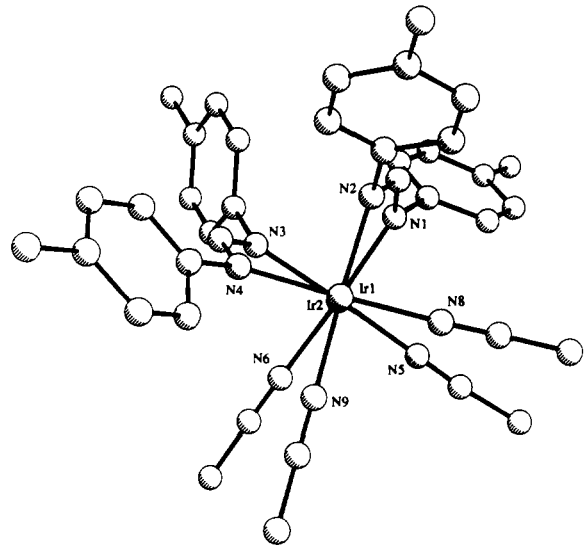

Fig. 3. View looking down the Ir–Ir axis of the cation in **3** that emphasizes the twist of the ligands from an eclipsed conformation. The axial acetonitrile ligands have been omitted for clarity.

Table 6
Torsion angles, χ (°), for **2**·$(CH_3)CO\cdot(C_2H_5)_2O$ and **3**

2·$(CH_3)_2CO\cdot(C_2H_5)_2O$	
Ir1–Ir2–N2–C15	28(2)
Ir1–Ir2–N4–C30	30(2)
Ir2–Ir1–N1–C15	27(2)
Ir2–Ir1–N3–C30	22(2)
3	
Ir1–Ir2–N2–C8	−21(1)
Ir1–Ir2–N4–C23	−22(1)
Ir2–Ir1–N1–C8	−19(1)
Ir2–Ir1–N3–C23	−18(1)
N6–Ir1–Ir2–N9	22.0(6)
N5–Ir1–Ir2–N8	20.4(5)

Table 6. The Ir–Ir distance in $[Ir_2(\mu\text{-form})_2(MeCN)_6]^{2+}$ is 2.601(1) Å, which is considerably shorter than the metal–metal distances in the afore-mentioned COD complexes with a dative Ir–Ir bond, but longer than the analogous distances in $Ir_2(\mu\text{-form})_4$ (2.524(3) Å) and the unusual compound $Ir_2(\mu\text{-}NC_5H_4)_2(\mu\text{-form})\text{-}(py)_2(MeCN)_2]^+$ with bridging orthometalated pyridine ligands (2.518(1) Å) [14]. Several factors are expected to contribute to a lengthening of the metal–metal distance in $[Ir_2(\mu\text{-form})_2(MeCN)_6]^{2+}$ as compared to $Ir_2(\mu\text{-form})_4$; these are (i) the presence of only two bridging ligands versus four, (ii) the cationic charge on the molecule which results in d orbital contraction and therefore reduced overlap, and (iii) the presence of axial ligands. The two axial acetonitrile ligands in **3** form much longer bonds to the Ir atoms than do the equatorial acetonitriles with average distances of Ir–N(ax) = 2.17(1) Å versus Ir–N(eq) = 2.00(1) Å. The average Ir–N(form) distance in **3** is 2.05(1) Å which is quite normal [13].

3.3. Spectroscopic and electrochemical measurements

3.3.1. NMR spectroscopy

^{1}H NMR spectra of the two compounds in CD_3CN are depicted in Fig. 4(a) and (b). The spectrum for **2** is rationalized on the basis of two magnetically inequivalent sets of tolylformamidinate ligands on the two Ir atoms; a mirror plane that bisects the bridgehead CH group relates the two nitrogen atoms and the tolyl groups on the same Ir atom, giving rise to C_s symmetry in solution. This is most easily discerned by examining the methyl region where two singlets appear at 2.33 and 2.29 ppm, and the aromatic region where four sets of doublets appear in the range 6.9–7.2 ppm. The magnetically equivalent CH groups give rise to a singlet at 7.90 ppm. Compound **3** displays a symmetrical pattern for the four tolylformamidinate groups as expected for a molecule of C_{2v} symmetry, with a singlet at 7.75 ppm for the N–CH–N groups, two doublets centered at 7.02 and 6.93 ppm for the aromatic protons and a singlet at 2.26 for the tolyl-CH_3 groups. Signals with the correct integration for two eq-MeCN ligands associated with **2** and four eq-MeCN ligands bound to **3** were observed, thus indicating the slow kinetics of exchange for these ligands. The axial MeCN ligands are in fast exchange, as judged by the presence of free MeCN at 1.95 ppm in both spectra.

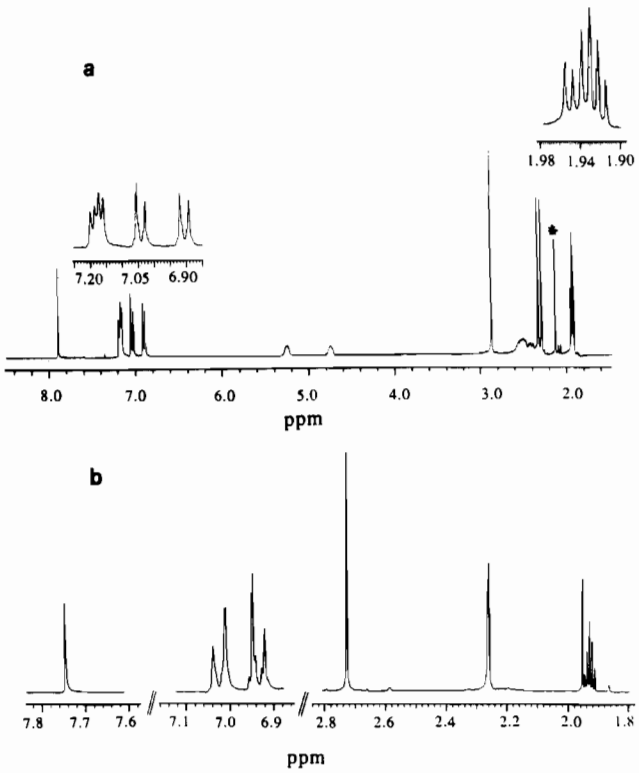

Fig. 4. 300 MHz ^{1}H NMR spectra of (a) **2** and (b) **3** in CD_3CN. In the spectrum of **2**, an H_2O impurity in the deuterated solvent is marked with an asterisk.

3.3.2. Electrochemistry

Cyclic voltammetric studies of **2** and **3** reveal dissimilar electronic properties, with **2** closely resembling the redox properties measured for the parent compound $Ir_2(COD)(\mu\text{-form})_2(O_2CCF_3)_2(H_2O)$ (**1**) [13]. Compound **1** was reported to exhibit an irreversible reduction at $E_{p,c} = -0.70$ V that is coupled with an oxidation wave at $E_{p,a} = -0.24$ V, and a quasi-reversible reduction at $E_{1/2}(\text{red}) = -1.37$ V versus Ag/AgCl. Compound **2**, whose cyclic voltammogram is displayed in Fig. 5(a), contains two MeCN ligands in place of the two η^1-O_2CCF_3 groups and displays an irreversible reduction at $E_{p,c} = -0.15$ V coupled with a wave at $E_{p,a} = +1.05$ V, a quasi-reversible reduction at $E_{1/2}(\text{red}) = -0.50$ V and a reversible oxidation at $E_{1/2}(\text{ox}) = +1.23$ versus Ag/AgCl. The absence of an observed oxidation for **1** is attributed to the fact that THF, which begins to oxidize at ~0.8 V was used as the solvent for the electrochemical investigation of **1** whereas acetone was used for the cyclic voltammetric measurements of **2**. Clearly the gross features of the two cyclic voltammograms are very similar; the shifts to less negative potentials for the reduction processes in **2** as compared to **1** may be explained in terms of the loss of the π-donor groups and the overall +2 charge on the molecule, both of which would contribute to more facile reduction. These electrochemical properties taken together with the different geometries of the two Ir centers observed in the crystal structure of **2** (vide supra) provide strong evidence for the description of **2** as a mixed-valence $Ir_2(I,III)$ species.

In contrast to the facile reductions exhibited by **2**, compound **3** reveals a single irreversible reduction at $E_{p,c} = -0.88$ V which is associated with a return wave at $E_{p,a} = -0.44$ V. A reversible oxidation occurs at $E_{1/2}(\text{ox}) = +0.77$ V versus Ag/AgCl (Fig. 5(b)). These electrochemical properties suggest that a redistribution of electrons has occurred with removal of the cyclo-

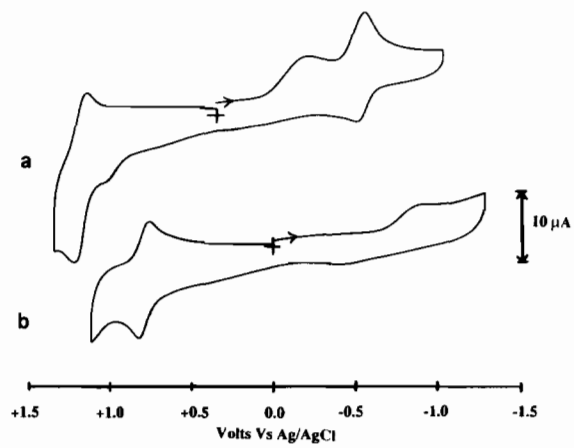

Fig. 5. Cyclic voltammograms of (a) **2** and (b) **3** in 0.15 M tetra-n-butylammonium hexafluorophosphate/$(CH_3)_2CO$ solution at a glassy carbon electrode and a scan rate of 200 mV s^{-1}.

octadiene ligand from **2** and that the resulting Ir_2^{4+} core is relatively stable.

4. Conclusions

The results of this study indicate that partially solvated cations of diiridium are accessible from the mixed-valence compound $Ir_2(COD)(\mu\text{-form})_2(O_2CCF_3)_2(H_2O)$. The isolation and full characterization of $[Ir_2(\mu\text{-form})_2(MeCN)_6]^{2+}$ with an Ir_2^{4+} core is a particularly promising development in the chemistry of Ir(II,II), as substitution of the four equatorial MeCN groups should allow access to a variety of compounds containing monodentate or bridging ligands. The possibility of preparing compounds of general type $Ir_2(\mu\text{-form})_2(\mu\text{-}O_2CR)_2$ is especially intriguing, as the Rh compound $Rh_2(\mu\text{-form})_2(\mu\text{-}O_2CCF_3)_2$ has been reported to be a highly active antitumor agent in studies involving *Yoshida acsites* sarcoma and the T8 sarcoma of Guerin in rats [22]. While the replacement of the remaining two formamidinate ligands by acetonitrile to give the fully solvated cation $[Ir_2(MeCN)_{10}]^{4+}$ has not yet been accomplished, it appears that acetonitrile is an excellent ligand for stabilizing singly bonded diiridium complexes, a fact that bodes well for the eventual isolation of the homoleptic solvated cation.

Acknowledgements

We gratefully acknowledge the National Science Foundation (Grant CHE-93-11812), the Camille and Henry Dreyfus Foundation and the Alfred P. Sloan Foundation for providing funding. The single crystal X-ray equipment was supported by the National Science Foundation (CHE-8403823 and CHE-8908088). NMR equipment was provided by the National Science Foundation (CHE-88-00770) and the National Institutes of Health (1-S10-RR04750-01). We thank Gary M. Finniss for assistance with cyclic voltammetric measurements.

References

[1] (a) J.M. Mayer and E.H. Abbott, *Inorg. Chem., 22* (1983) 2774; (b) F.A. Cotton and K.J. Wiesinger, *Inorg. Chem., 30* (1991) 871.
[2] F.A. Cotton, S.C. Haefner, C.J. Burns, A.K. Burrell and A.P. Sattelberger, *Division of Inorganic Chemistry, 207th ACS National Meet., San Diego, CA, Mar. 13–17, 1994,* Abstr. 246.
[3] S.N. Bernstein and K.R. Dunbar, *Angew. Chem., Int. Ed. Engl., 31* (1992) 1359.
[4] (a) K.R. Dunbar, *J. Am. Chem. Soc., 110* (1988) 8247; (b) L.M. Dikareva, V.I. Adrianov, A.N. Zhilyaev and I.B. Baranovskii, *Russ. J. Inorg. Chem. (Engl. Transl.), 34* (1989) 240; (c) K.R. Dunbar and L.E. Pence, *Inorg. Synth., 29* (1992) 182.
[5] (a) S.L. Bartley, S.N. Bernstein and K.R. Dunbar, *Inorg. Chim. Acta, 213* (1993) 213; (b) K.R Dunbar, L.E. Pence and J.L.C. Thomas, *Inorg. Chim. Acta, 217* (1994) 79; (c) K.R. Dunbar, *J. Cluster Sci., 5* (1994) 125; (d) D.E. Morris, S.K. Doorn, C.A. James, C.A. Arrington, K.R. Dunbar, G.M. Finniss, L.E. Pence and W.H. Woodruff, *J. Am. Chem. Soc.,* submitted for publication; (e) K.R. Dunbar and G.M. Finniss, unpublished results.
[6] F.A. Cotton and R. Poli, *Polyhedron, 6* (1987) 1625.
[7] A.W. Maverick, T.P. Smith, E.F. Maverick and H.B. Gray, *Inorg. Chem., 26* (1987) 4336.
[8] P.G. Rasmussen, J.E. Anderson, O.H. Bailey, M. Tamres and J.C. Bayón, *J. Am. Chem. Soc., 107* (1985) 279.
[9] K.J. Del Rossi and B.B. Wayland, *J. Chem. Soc., Chem. Commun.,* (1986) 1653.
[10] J.J. Bonnet, A. Thorez, A. Maisonnat, J. Glay and R. Poilblanc, *J. Am. Chem. Soc., 101* (1979) 5940.
[11] (a) J.V. Caspar and H.B. Gray, *J. Am. Chem. Soc., 106* (1984) 3029; (b) R.D. Brost and S.R. Stobart, *Inorg. Chem., 28* (1989) 4307, and refs. therein.
[12] F.A. Cotton and R.A. Walton, *Multiple Bonds Between Metal Atoms,* Oxford University Press, Oxford, UK, 2nd edn., 1993, Ch. 8, pp. 502–507.
[13] F.A. Cotton and R. Poli, *Inorg. Chem., 26* (1987) 590.
[14] F.A. Cotton and R. Poli, *Organometallics, 6* (1987) 1743.
[15] R.M. Roberts, *J. Org. Chem., 14* (1949) 277.
[16] (a) A. Bino, F.A. Cotton and P.E. Fanwick, *Inorg. Chem., 18* (1979) 3558; (b) F.A. Cotton, B.A. Frenz, G. Deganello and A. Shaver, *J. Organomet. Chem.,* (1973) 227.
[17] *TEXSAN–TEXRAY Structure Analysis Package,* Molecular Structure Corporation, The Woodlands, TX, 1985.
[18] R.X. Fischer and E. Tillmanns, *Acta Crystallogr., Sect. C, 44* (1988) 775–776.
[19] C.J. Gilmore, *J. Appl. Crystallogr., 17* (1984) 42.
[20] R.T. Beurskens, DIRDIF: direct methods for difference structure, an automatic procedure for phase extension; refinement of difference structure factors, *Tech. Rep. 1984/1,* Crystallography Laboratory, Toernooiveld, Nijmegen, Netherlands, 1984.
[21] N. Walker and D. Stuart, *Acta Crystallogr., Sect. A, 39* (1983) 158–166.
[22] V. Fimiani, T. Ainis, A. Cavallaro and P. Piraino, *J. Chemother., 2* (1990) 319.